JTAM (Jurnal Teori dan Aplikasi Matematika)
http://journal.ummat.ac.id/index.php/jtam
p-ISSN 2597-7512 | e-ISSN 2614-1175
Vol. 10, No. 2, April 2026, pp. 378-395

Comparing Areal and Grid Supports for Fire Radiative Power within a GSTAR (p; λ_1, λ_2, ..., λ_p) Framework

Zuleha[1], Nur'ainul Miftahul Huda[1*], Nurfitri Imro'ah[2]
[1]Mathematics Department, Universitas Tanjungpura, Indonesia
[2]Statistics Department, Universitas Tanjungpura, Indonesia
nurainul@fmipa.untan.ac.id

Article History:
Received : 22-11-2025
Revised : 17-01-2026
Accepted : 19-01-2026
Online : 01-04-2026

Keywords:
Spatial-Temporal;
GSTAR;
Grid;
Weight Matrix;
FRP.

ABSTRACT

Forest fire phenomena exhibit spatial interdependence and temporal dependence, necessitating a spatiotemporal modeling approach to capture the dynamics of fire occurrences. This study models and predicts forest fires using Fire Radiative Power (FRP) as an indicator of fire intensity. Weekly hotspot data from NASA FIRMS, covering the period from July 2024 to August 2025, were analyzed using the Generalized Space-Time Autoregressive (GSTAR) model. The modeling was conducted by considering various forms of spatial partitioning and spatial weight matrices to capture inter-location dependencies. Four spatial partitioning schemes were employed: areal, and grids of 0.50° × 0.50°, 1.00° × 1.00°, and 1.25° × 1.25°; alongside three spatial weight matrices: Queen Contiguity, Rook Contiguity, and Inverse Distance Weighting (IDW). The temporal order and spatial lag were determined using STACF and STPACF plots. From these combinations, 42 GSTAR models were constructed and evaluated through a three-stage process of estimation and residual diagnostic testing. The results indicate that the GSTAR (1;1) model with a 1.00° × 1.00° grid and Rook Contiguity and IDW spatial weight matrices is the best-performing model. This model satisfies the white noise assumption and yields a Root Mean Square Error (RMSE) of 6.866, which is the smallest among all evaluated models. The estimates indicate that fires at a given location are influenced by prior conditions and spatial interactions with surrounding areas, suggesting that the GSTAR model supports spatiotemporal monitoring and early warning systems.

https://doi.org/10.31764/jtam.v10i2.36663

A. INTRODUCTION

The Generalized Space-Time Autoregressive (GSTAR) model is an extension of the Space-Time Autoregressive (STAR) model and the AutoRegressive (AR) model, integrating spatial and temporal dependencies simultaneously (Hestuningtias & Kurniawan, 2023; Nurhayati et al., 2025; Pratiwi et al., 2025; Yundari et al., 2025). GSTAR is used to analyze geographically distributed time series data by accounting for temporal dependence (the Influence of past values) and spatial dependence (the Influence of neighboring locations) (Huda et al., 2023; Huda & Imro'ah, 2024). In the GSTAR framework, the value of a variable at a specific location and time is influenced not only by its past values at that location but also by the values of the variable at neighboring locations, both contemporaneously and at prior time points. This property allows GSTAR to simultaneously capture spatial interactions and temporal dynamics, making it suitable for modeling phenomena that evolve across space and time (Huda et al., 2023; Pasaribu et al., 2022). In the application of GSTAR, the study area is divided into spatial units,

which can be square grids generated through a gridding process or areal units defined by administrative boundaries (Ayyash et al., 2025; Imro'ah et al., 2025).

Each spatial unit represents a single observational location within the model. The relationships between spatial units are represented through a spatial weight matrix, which quantifies the degree of connectivity and Influence among locations (Ayyash et al., 2025; Huda & Imro'ah, 2023; Mukhaiyar et al., 2024; Utami et al., 2024; Yundari et al., 2018). Spatial weight matrices are typically constructed based on geographic proximity, shared boundaries, or inter-location distances. Through this weighting structure, spatial interactions are systematically incorporated into the GSTAR modeling process. The selection of spatial units and the design of spatial weight matrices significantly affect the accuracy of GSTAR modeling. A well-defined weighting structure enables the model to accurately represent interregional interactions, thereby improving estimation and prediction outcomes (Ayyash et al., 2025; Huda & Imro'ah, 2023; Mukhaiyar et al., 2021; Utami et al., 2024; Yundari et al., 2018). GSTAR has been widely applied across various environmental fields, particularly for phenomena requiring predictions across multiple locations and time periods. Examples include rainfall forecasting (Aprianti et al., 2024), the spread of infectious diseases (Huda & Imro'ah, 2024; Pasaribu et al., 2021), the analysis of agricultural commodity price fluctuations affected by climate factors (Yundari et al., 2025), and the monitoring and prediction of forest fires in neighboring regions (Ayyash et al., 2025; Mukhaiyar et al., 2024; Pratiwi et al., 2025).

Forest fires in Indonesia represent a spatial-temporal phenomenon with wide-ranging impacts on the environment and society. Fire occurrences exhibit spatial dependence among adjacent regions, both in hotspot emergence and in the spread of impacts. Consequently, modeling forest fires requires an approach that captures both spatial interactions and temporal dynamics simultaneously. One key indicator used in monitoring forest and land fires is Fire Radiative Power (FRP), which measures the thermal energy emitted by hotspots in megawatts (MW) (Kusuma et al., 2017). FRP values are closely related to the amount of biomass burned and serve as indicators of fire intensity, making them highly relevant for spatial-temporal modeling. West Kalimantan Province is particularly prone to forest and land fires due to the predominance of peatlands. Peatlands store large amounts of biomass and are highly flammable when dried or physically disturbed (Ayyash et al., 2025). Fire occurrences in this region are generally associated with land-use changes, such as agricultural and plantation development, and are influenced by climatic conditions, including drought periods and El Niño events (Omar et al., 2022; Pratiwi et al., 2025). The impacts of fires extend beyond ecosystem damage to include public health risks from smoke and disruptions to economic and social activities (Cahyono et al., 2015; Jalilov et al., 2025).

Previous studies have demonstrated the applicability of GSTAR in forest fire modeling. However, most have been limited to using a single type of spatial unit either grids or administrative areal units and a single type of spatial weight matrix. Comparative analyses that examine both areal and grid-based spatial divisions across multiple grid sizes, combined with different types of spatial weight matrices within a single GSTAR framework, remain scarce. Furthermore, the use of FRP as an indicator of fire intensity in comparative analyses that vary across spatial units and spatial weight matrices, particularly in peatland areas of West Kalimantan Province that are highly susceptible to fire, warrants further investigation. This

situation underscores the need for a more comprehensive study to achieve a more accurate and representative understanding of forest fire dynamics using the GSTAR model.

Based on these considerations, this study aims to analyze the accuracy of the GSTAR model across four spatial divisions: areal units and grids of sizes $0.50° \times 0.50°$, $1.00° \times 1.00°$, and $1.25° \times 1.25°$, combined with three types of spatial weight matrices: Queen Contiguity, Rook Contiguity, and Inverse Distance Weight (IDW). The study area covers 14 sub-districts across the Regencies of Sanggau, Sekadau, and Ketapang in West Kalimantan Province. These three regencies are considered highly prone to forest fires, particularly during the dry season, underscoring the need for spatial-temporal analysis to understand hotspot distribution patterns and predict regions with high fire risk. The application of the GSTAR framework in this study is expected to identify the most accurate combination of spatial units and spatial weight matrices for predicting the distribution of forest fire hotspots in the region.

B. METHODS

1. Generalized Space Time Autoregressive (GSTAR) Model

The GSTAR model was first introduced by Borovkova, Lopuha, and Ruchjana in 2002. It was developed to analyze time-series data characterized by heterogeneous spatial variation. (Ayyash et al., 2025). The main distinction lies in the autoregressive parameters of the GSTAR model, which are allowed to vary across different locations (Umer et al., 2018). The GSTAR model has a wide range of applications, including environmental studies for mapping disease distribution and analyzing climate change. Systematically, the GSTAR $(p; \lambda_1, \lambda_2, \dots, \lambda_p)$model can be expressed as follows (Huda & Imro'ah, 2023; Pasaribu et al., 2018; Pratiwi et al., 2025).

$$\boldsymbol{Y}_t = \left(\sum_{k=1}^{p} \sum_{\ell=0}^{\lambda_k} \boldsymbol{\Phi}_{k\ell} \boldsymbol{W}^{(\ell)} \boldsymbol{Y}_{t-k} \right) + \boldsymbol{e}_t \tag{1}$$

where $\boldsymbol{Y}_t = \left[Y_t^{(1)}, Y_t^{(2)}, \dots, Y_t^{(N)} \right]^{\top}$ is the observation vector at time t, $\boldsymbol{\Phi}_{k\ell} = diag\,(\phi_{k\ell}^{(1)}, \phi_{k\ell}^{(2)}, \dots, \phi_{k\ell}^{(N)})$ denotes the autoregressive coefficient matrix $\boldsymbol{W}^{(\ell)}$represents the spatial weight matrix at the ℓ spatial order, and $\boldsymbol{e}_t = [e_t^{(1)}, e_t^{(2)}, \dots, e_t^{(N)}]^{\top}$is the error vector.

2. Spatio-Temporal Weight Structure in the GSTAR Model $(\boldsymbol{p}; \boldsymbol{\lambda_1}, \boldsymbol{\lambda_2}, \dots, \boldsymbol{\lambda_p})$

In this study, three types of spatial weight matrices are employed, namely the Queen Contiguity, Rook Contiguity, and Inverse Distance Weight (IDW) matrices. The Queen and Rook Contiguity weight matrices represent spatial lag based on neighbourhood relationships between regions. In contrast, the IDW weight matrix represents spatial lag based on inter-regional relationships within a specified distance radius. Accordingly, the spatial weight matrices used in this study can be classified into two categories:

a. Neighbors

The neighborhood-based spatial weight matrix represents proximity relationships among observation locations. This matrix is defined as an $N \times N$ matrix, where N denotes the number of locations, and is expressed as (Pratiwi, Imro'ah, Huda, et al., 2025):

$$\boldsymbol{W}^{(\ell)} = \left[w_{ij}^{(\ell)}\right]_{N\times N} \tag{2}$$

with the conditions $w_{ii}^{(\ell)} = 0$ and $\sum_{j=1,j\neq i}^{N} w_{ij}^{(\ell)} = 1$. Each element $w_{ij}^{(\ell)}$ describes the relative influence or interaction strength between the j^{th} and i^{th} locations at spatial lag ℓ, ensuring that the total influence on each spatial unit is standardized. Furthermore, the neighborhood-based spatial weight matrix is normalized so that each row's weights sum to 1. This row normalization is performed by dividing each weight by the sum of the weights in the corresponding row, resulting in the normalized spatial weight matrix as follows:

$$\boldsymbol{W}^{(\ell)} = \left[w_{ij}^{(\ell)}\right] = \left[\frac{w_{ij}^{(\ell)}}{\sum_{j=1,j\neq i}^{N} w_{i}^{(\ell)}}\right]_{N\times N} \tag{3}$$

b. Queen Contiguity

The Queen contiguity weight matrix is a method for defining neighbourhood relationships that is broader and more flexible. In Queen contiguity, two locations are considered neighbours if they share either a common edge or a common corner (Huda & Imro'ah, 2023; Pratiwi, Imro'ah, Huda, et al., 2025). This matrix is used because forest fire interactions are not limited to direct boundary sharing but may also occur through diagonal adjacency, making Queen contiguity more suitable for capturing broader spatial dependence. This can be observed in Figure 1, which presents the structure of the Queen contiguity spatial weight matrix for both areal and grid representations. In the illustration, the dark green colour indicates the spatial objects that represent the study locations.

(a) (b)

(c) (d)

Figure 1. Ilustration of Queen Contiguity: (a) Areal with spatial lag 1, (b) Areal with spatial lag 2, (c) Grid with spatial lag 1, (d) Grid with spatial lag 2

c. Rook Contiguity

The Rook contiguity weight matrix considers only locations that share a common edge (top, bottom, left, and right) and does not account for corners (Ayyash et al., 2025; Purwaningsih et al., 2025). This matrix is used to emphasize direct, immediate spatial interactions by restricting neighbourhood relationships to side-sharing boundaries, thereby capturing more localized spatial dependence. As illustrated in Figure 2, the resulting neighbourhood structure is more limited than that of the Queen contiguity. In particular, Figures 2(a) and 2(b) exhibit an identical neighbourhood configuration to Figures 1(a) and 1(b), as all areal units share boundaries along their sides; the dark green colour denotes the spatial objects representing the study locations.

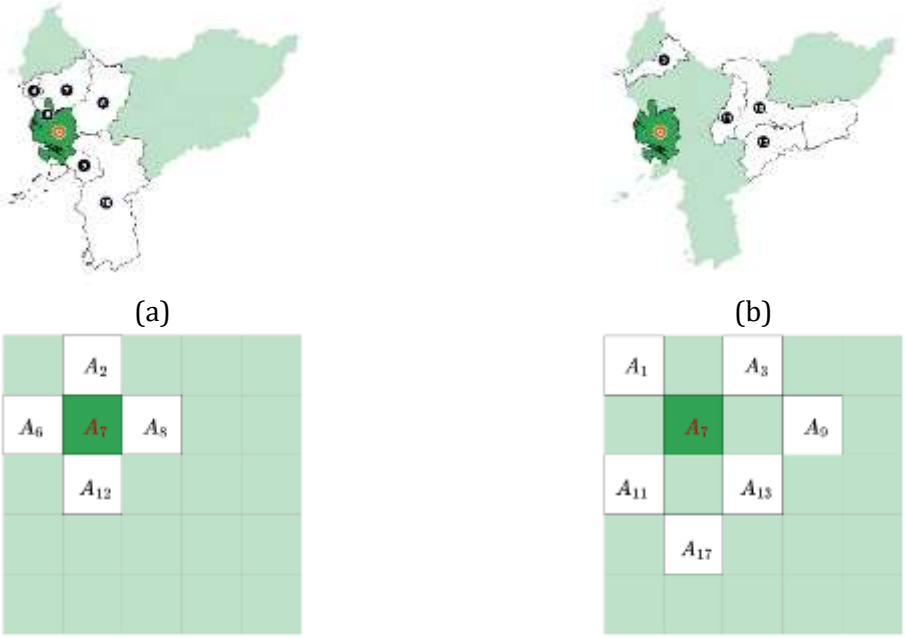

(a) (b)

(c) (d)

Figure 2. Ilustration of Rook Contiguity: (a) Areal with spatial lag 1, (b) Areal with spatial lag 2, (c) Grid with spatial lag 1, (d) Grid with spatial lag 2

d. Distance

Based on distance, the weight matrix is constructed using travel distances or distances between locations within a study area. Spatial relationships among observation locations are determined using the geographical distance between locations. In this approach, the spatial Influence of a location is restricted to a specified radius, so that only locations within that radius are considered to have spatial interactions (Mubarak et al., 2021). To represent a distance-based spatial lag, an Inverse Distance Weight (IDW) spatial weight matrix is employed. In this matrix, spatial weights are constructed as the inverse of the distance between locations, implying that locations located closer to each other exert greater Influence than those farther apart. Locations outside the specified radius are assigned a weight of 0 and are assumed to have no spatial Influence (Notonegoro et al., 2024). In general, the IDW spatial weight matrix at spatial lag ℓ can be expressed as (Huda et al., 2021, 2023):

$$\boldsymbol{W}^{(\ell)} = \left[w_{ij}^{(\ell)}\right] = \left[\frac{\frac{1}{d_{ij}^{(\ell)}}}{\sum_{j=1, j\neq i}^{N} \frac{1}{d_{ij}^{(\ell)}}}\right]_{N\times N} \tag{4}$$

where d_{ij}represents the distance between location j^{th} and i^{th}.

This matrix is employed because the spatial Influence of forest fires tends to decrease with distance, making IDW approach appropriate for capturing continuous, distance-based spatial dependence. In this approach, the spatial Influence of a location is constrained by a specified distance radius, such that only locations within this radius are considered in constructing spatial relationships. For the IDW spatial weight matrix, the spatial relationships among locations are shown in Figure 3, which illustrates the interactions among nearby locations within the defined radius. In the illustration, the dark green color represents the spatial objects corresponding to the study locations.

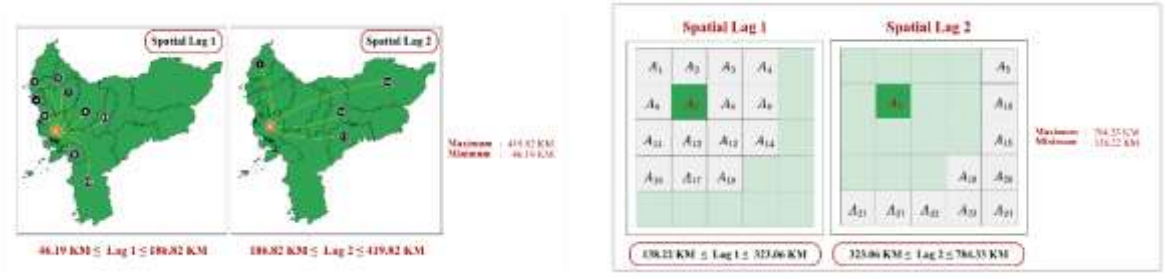

(a) (b)

Figure 3. Illustration of radius-based spatial lag: (a) areal with spatial lag 1, (b) areal with spatial lag 2, (c) grid with spatial lag 1, (d) grid with spatial lag 2

3. Parameter Estimation

The Ordinary Least Squares (OLS) method is employed to estimate the parameters of the GSTAR model. This method aims to determine parameter values that minimize the difference between observed and predicted values, while accounting for both spatial and temporal dependencies in the model. Mathematically, the OLS method can be expressed as follows (Abdullah et al., 2018; Pratiwi, Imro'ah, & Huda, 2025).

$$\boldsymbol{Y} = \boldsymbol{X\Phi} + \boldsymbol{e} \tag{5}$$

Equation (5) can also be expressed in the context of the GSTAR (1;1) model.

where $\boldsymbol{Y} = \left[Y_t^{(1)}, Y_t^{(2)}, \ldots, Y_t^{(N)}\right]^{\top}$, $\boldsymbol{e_t} = \left[e_t^{(1)}, e_t^{(2)}, \ldots, e_t^{(N)}\right]^{\top}$ and The parameter vector $\boldsymbol{\Phi}$ contains the autoregressive coefficients that represent both the local temporal effects and the spatial influences for each location. The matrix $\boldsymbol{X}$ represents the explanatory variables that combine both temporal and spatial lag values from all locations, and can be written as:

$$\boldsymbol{X_{(t-1)}} = \begin{bmatrix} Y_{(t-1)}^{(1)} & V_{(t-1)}^{(1)} & \cdots & \cdots & 0 & 0 \\ 0 & 0 & \cdots & \cdots & 0 & 0 \\ 0 & 0 & \ddots & \ddots & \vdots & \vdots \\ 0 & 0 & \cdots & \cdots & Y_{(t-1)}^{(N)} & V_{(t-1)}^{(N)} \end{bmatrix} \tag{6}$$

The component $V_{(t-1)}^{(i)}$ in the matrix above denotes the spatial influence from other locations on the i^{th} location, and is defined as: $V_{(t-1)}^{(i)} = \sum_{j=1, j\neq i}^{N} w_{ij} Y_{(t-1)}^{(j)}$. Hence, each location is affected by its own past values as well as by the weighted combination of its neighboring locations, based on the spatial weight matrix $\boldsymbol{W} = [w_{ij}]_{N\times N}$. Thus, Equation (5) can be used for parameter estimation (Setiawan et al., 2016).

$$\widehat{\boldsymbol{\Phi}} = [\boldsymbol{X^T X}]^{-1}[\boldsymbol{X^T Y}] \tag{7}$$

In general, the stages of this study include order identification, parameter estimation, residual diagnostics, and forecasting. The flowchart in Figure 4 provides a more detailed illustration of the stages involved in constructing the GSTAR model from hotspot data.

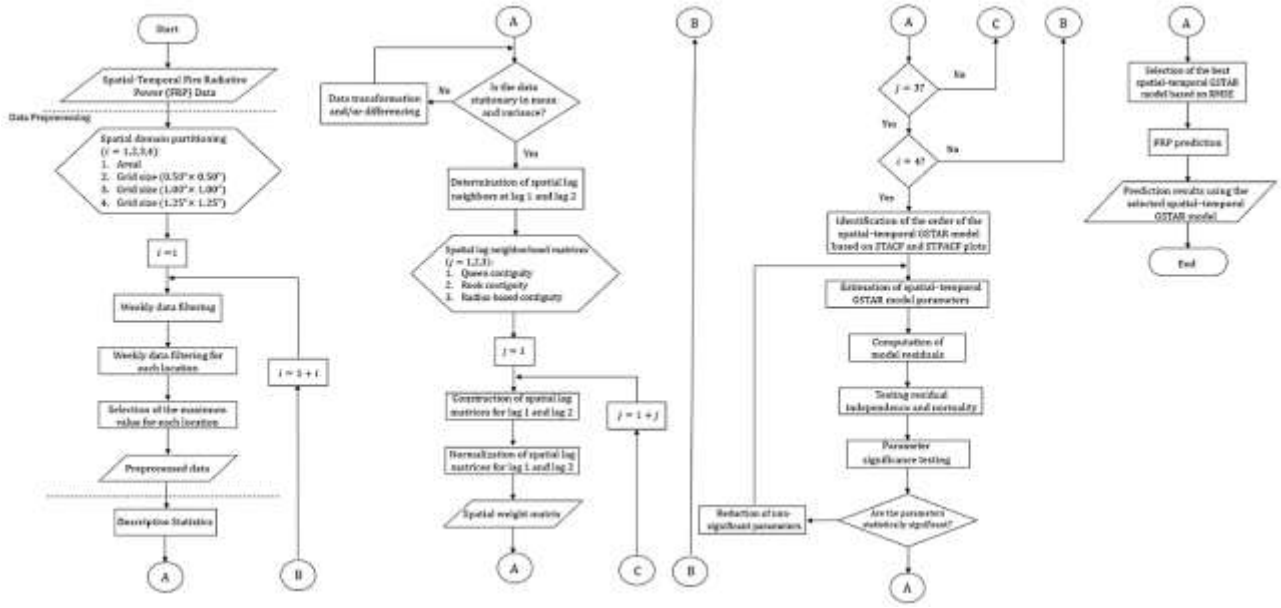

Figure 4. Flowchart of GSTAR Model

C. RESULT AND DISCUSSION

1. Data Preprocessing

Data preprocessing was conducted to ensure that the data used for constructing the GSTAR model met the fundamental assumptions and were ready for analysis. The data consisted of weekly FRP Fire Radiative Power (FRP) values derived from hotspot observations obtained from the Fire Information for Resource Management System (NASA FIRMS) website (NASA-FIRMS, 2025). Covering the period from July 2024 to August 2025. The dataset included information on date, longitude, latitude, and FRP values.

Research in West Kalimantan covered three regencies, namely Ketapang, Sanggau, and Sekadau (see Figure 5(a)). The selection of these regencies was based on hotspot data obtained from the official website of the Ministry of Environment and Forestry (sipongi.menlhk.go.id, 2025). Sanggau Regency recorded the highest number of hotspots, followed by Ketapang, while Sekadau was included because it borders both regencies and displays a similar hotspot distribution pattern. In total, 14 districts were used as the spatial units of analysis (see Figure 5(c)). These districts were selected due to their high hotspot occurrences and spatial interconnectedness. Of these, nine districts are located in Ketapang Regency, two in Sanggau Regency, and three in Sekadau Regency. The distribution of hotspot intensity across the three regencies is presented in Figure 5.

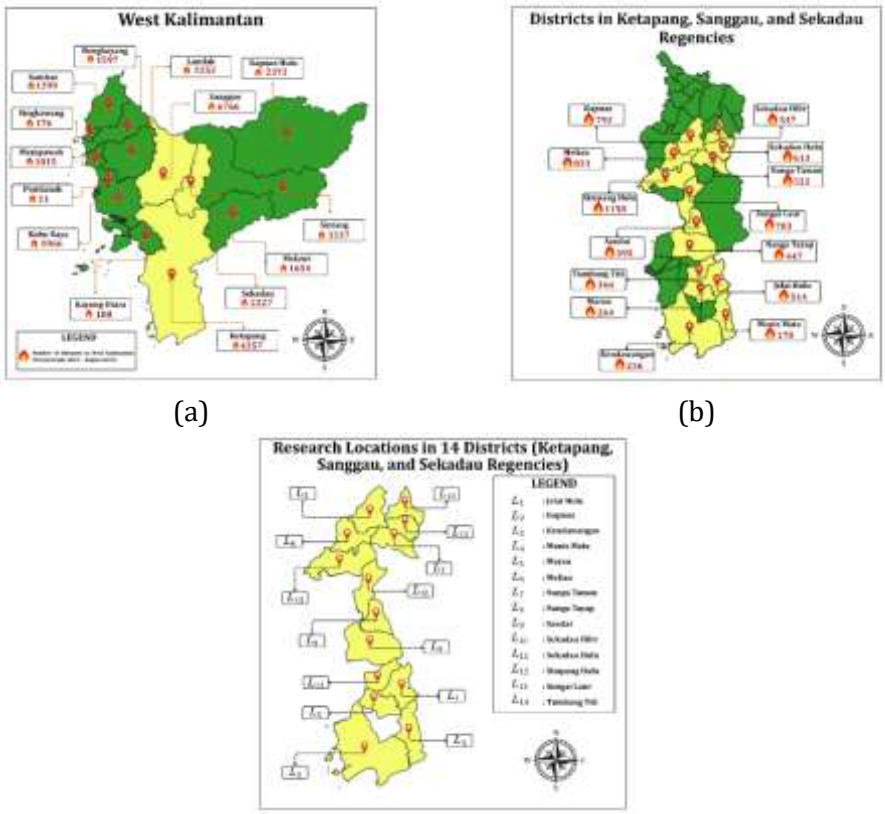

(a) (b)

(c)

Figure 5. (a) Number of forest fire hotspots, (b) District boundaries in Ketapang, Sanggau, and Sekadau Regencies, (c) study areas, where the yellow areas represent the regions analyzed in this study, and the labels $\boldsymbol{L_1 - L_{14}}$ indicate the $\boldsymbol{i^{th}}$ location shown in the map

After identifying the target locations for analysis, namely 14 districts as the spatial units of analysis (see Figure 5(c)), these areas were then transformed into spatial representations using three different grid sizes: $0.50° \times 0.50°$, $1.00° \times 1.00°$, and $1.25° \times 1.25°$ (see Figure 6).

(a) (b) (c)

Figure 6. Spatial grid representations of the study area at different supports: (a) $\boldsymbol{0.50° \times 0.50°}$, (b) $\boldsymbol{1.00° \times 1.00°}$, (c) $\boldsymbol{1.25° \times 1.25°}$

After the grids were generated, hotspot data from both the areal and grid systems were filtered and combined into 61 weekly observations, with each observation representing the maximum FRP value. The representative value for each unit was defined as the highest FRP

detected, or zero if no fire was present, allowing for a consistent analysis of fire intensity across space and time.

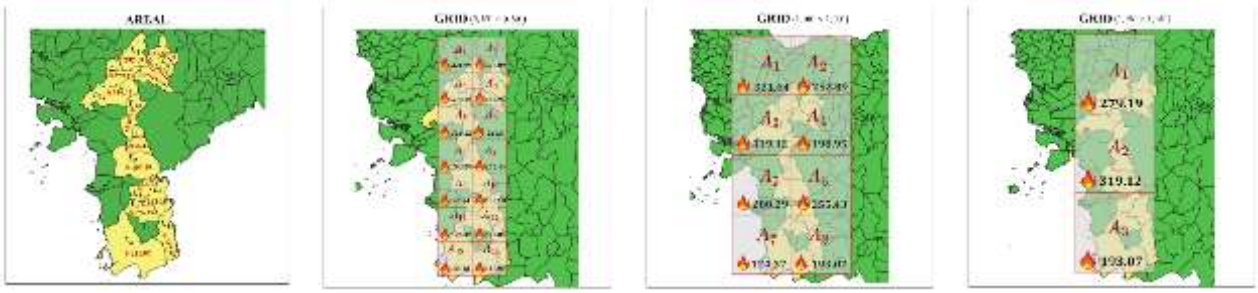

Figure 7. Selection of the maximum value for each location

2. Numerical Summary

After the data collection process was completed, a descriptive statistical analysis was performed to provide an overview of the spatial and temporal distribution of forest fire hotspots during the study period (Ray et al., 2023). This analysis employed fundamental statistical indicators such as mean, standard deviation, and maximum value to describe the variability and central tendency of hotspot occurrences across all spatial units. The dataset was categorised into four types of spatial representations, namely areal and three grid supports: $0.50° \times 0.50°$, $1.00° \times 1.00°$, and $1.25° \times 1.25°$. In total, 61 observations were included, covering the period from July 2024 to August 2025, with each observation representing the number of hotspots detected at a specific spatial location. The resulting descriptive statistics provide an overview of the hotspot distribution across the four spatial representations. A summary of the descriptive analysis results is presented in Table 1.

Table 1. Descriptive statistics of FRP across areal and grid supports for the period from July 2024 to August 2025

Descriptive Statistic	**Areal**													
	L_1	L_2	L_3	L_4	L_5	L_6	L_7	L_8	L_9	L_{10}	L_{11}	L_{12}	L_{13}	L_{14}
Mean	15.3	16.6	10.5	9.7	12.2	**25.7**	13.1	10.1	18.8	11.6	15.3	16.3	15.3	16.6
Maximum	133.2	252.1	111.0	193.1	124.4	279.2	145.9	107.6	255.4	182.5	199.0	**319.1**	280.1	55.5
Std. Dev.	27.5	42.0	17.4	26.3	25.2	**50.3**	30.6	20.1	43.2	28.8	37.1	46.5	46.1	14.6
Grid $0.50° \times 0.50°$														
	A_1	A_2	A_3	A_4	A_5	A_6	A_7	A_8	A_9	A_{10}	A_{11}	A_{12}	A_{13}	A_{14}
Mean	**24.5**	17.3	29.5	22.4	22.3	8.6	18.3	16.1	7.6	11.5	11.2	19.7	5.3	8.2
Maximum	222.0	252.1	279.2	199.0	**319.1**	126.5	280.3	255.4	49.5	133.2	124.4	193.1	33.4	111.0
Std. Dev.	47.6	39.9	**53.5**	44.5	51.1	21.8	43.9	41.1	11.9	23.3	47.6	39.9	**53.5**	44.5
Grid $1.00° \times 1.00°$									**Grid $1.25° \times 1.25°$**					
	A_1	A_2	A_3	A_4	A_5	A_6	A_7	A_8	A_1	A_2	A_3	-	-	-
Mean	**46.2**	26.8	39.3	26.9	21.2	23.3	13.3	24.8	**46.8**	30.6	29.4	-	-	-
Maximum	**321.6**	252.1	319.1	199.0	280.3	255.4	124.4	193.1	279.2	**319.1**	193.1	-	-	-
Std. Dev.	**74.3**	51.0	66.5	48.2	43.7	44.4	21.8	35.2	**67.5**	54.6	37.8	-	-	-

The descriptive statistics summarised in Table 2 highlight the spatial patterns of fire intensity across different support levels. The **bold black** values represent the highest mean values at each support level, identified in L_6 at the areal level, A_1 at the $0.50° \times 0.50°$ grid, A_1 at the $1.00° \times 1.00°$ grid, and A_1 at the $1.25° \times 1.25°$ grid. These indicate that the regions corresponding to L_6 and A_1 consistently exhibit the highest average fire intensity, suggesting

relatively frequent and stable fire activities in those areas. The **red** values denote the maximum values, indicating the locations with the most intense fire events during the observation period July 2024–August 2025. These are found at L_{12} for the areal level, A_5 for the 0.50° × 0.50° grid, A_1 for the 1.00° × 1.00° grid, and A_2 for the 1.25° × 1.25° grid. This suggests that these areas experienced the strongest fire episodes, reflected by the highest fire radiative power among all locations at their respective supports. Meanwhile, the **blue** values indicate the highest standard deviation, reflecting the most significant fluctuation or instability in fire intensity. These occur at L_6 for the areal level, A_3 and A_{13} for the 0.50° × 0.50° grid, as well as A_1 for the 1.00° × 1.00° grid and A_1 for the 1.25° × 1.25° grid. This implies that fire intensity in these regions was highly variable over time, indicating fluctuating fire activity levels throughout the observation period.

3. Data Stationarty Test

The stationarity test is a fundamental step before conducting time series modelling. Stationarity refers to the statistical stability of a dataset, wherein its mean and variance remain constant over time. A time series is considered stationary when its fluctuations occur around a constant mean with a uniform variance (Pusporani et al., 2024). The Augmented Dickey-Fuller (ADF) test was subsequently applied to verify the data's stationarity (Roza et al., 2022). The results revealed that the p-value for all areal and grid types was 0.01, which is below the 0.05 significance threshold. Consequently, the data for all areal and grid types were confirmed to exhibit stationarity.

4. Spatial Weight Matrix

In this study, three types of spatial weighting were used, namely Queen Contiguity, Rook Contiguity, and Inverse Distance Weight (IDW). The model was constructed by considering lag 1 and lag 2 to capture spatial and temporal dependencies between locations. The analysis was conducted on areal units and three grid sizes, namely 0.50° × 0.50°, 1.00° × 1.00°, and 1.25° × 1.25°. The approximate spatial distances for these grid sizes are $\mathbf{55.5\ KM\ for\ 0.50° \times 0.50°}$, $\mathbf{111\ KM\ for\ 1.00° \times 1.00°}$, and $\mathbf{138.75\ KM\ for\ 1.25° \times 1.25°}$. Examples of the spatial weight matrices used in this study are presented in Table 2, including the Queen weight matrix for areal representation, the 0.50° × 0.50° grid for Rook Contiguity, and the 1.25° × 1.25° grid for IDW, each represented by a specific symbol W_{q} (Pratiwi, Imro'ah, Huda, et al., 2025), W_{r} (Purwaningsih et al., 2025), and W_{i} (Huda et al., 2021).

Table 2. Spatial Weight Matrix: Queen Contiguity, Rook Contiguity, and Inverse Distance Weighting (IDW)

	Spatial Weight Matrix		
	Ilustration	$\boldsymbol{W^{(1)}}$	$\boldsymbol{W^{(2)}}$
	Queen Contiguity ($\mathbf{W_q}$)		
Areal		$\begin{bmatrix} 0 & 0 & \cdots & 0.33 \\ 0 & 0 & \cdots & 0 \\ 0 & 0 & \cdots & 0 \\ 0.33 & 0 & \cdots & 0 \\ \vdots & \vdots & \ddots & \vdots \\ 0.33 & 0 & \cdots & 0 \end{bmatrix}$	$\begin{bmatrix} 0 & 0 & \cdots & 0 \\ 0 & 0 & \cdots & 0 \\ 0.5 & 0 & \cdots & 0.5 \\ 0 & 0 & \cdots & 0 \\ \vdots & \vdots & \ddots & \vdots \\ 0 & 0 & \cdots & 0 \end{bmatrix}$
⋮	⋮	⋮	⋮
	Inverse Distance Weight ($\boldsymbol{W_i}$)		
Grid ($1.25° \times 1.25°$)		$\begin{bmatrix} 0 & 1 & 0 \\ 0.5 & 0 & 0.5 \\ 0 & 1 & 0 \end{bmatrix}$	Grid cell A2 has no second-order neighbors in this spatial grid, indicating that grid cell A2 has no second-order spatial locations in any direction. Therefore, it is not possible to construct an exact queen contiguity weight matrix.

5. Parameter Estimation and Diagnostics Residual Test

A total of **42 models** were used in this study, derived from the combination of four GSTAR model structures GSTAR (1;1), GSTAR (2;1), GSTAR (1;1,2), and GSTAR (2;1,2) for the areal representation and the $0.50° \times 0.50°$ and $1.00° \times 1.00°$ grids. For the $1.25° \times 1.25°$ grid, only the GSTAR (1;1) and GSTAR (2;1) models were applied because this grid does not support second order spatial. Each spatial representation was further combined with three spatial weighting schemes, namely Queen Contiguity, Rook Contiguity, and Inverse Distance Weight (IDW), resulting in a total of 42 model configurations analyzed in this study. Based on Equation (1), these four GSTAR structures were used to capture spatial and temporal dependencies through spatial weight matrices $\boldsymbol{W^{(\ell)}}$, which represents the relationships between regions. The general forms of the models are expressed as follows.

$$\text{GSTAR}(1;1) \quad : \boldsymbol{Y}_t = \boldsymbol{\Phi}_{10}\boldsymbol{Y}_{(t-1)} + \boldsymbol{\Phi}_{11}\boldsymbol{W}^{(1)}\boldsymbol{Y}_{(t-1)} + \boldsymbol{e}_t \tag{8}$$

$$\text{GSTAR}(2;1) \quad : \boldsymbol{Y}_t = \boldsymbol{\Phi}_{10}\boldsymbol{Y}_{(t-1)} + \boldsymbol{\Phi}_{11}\boldsymbol{W}^{(1)}\boldsymbol{Y}_{(t-1)} + \boldsymbol{\Phi}_{20}\boldsymbol{Y}_{(t-2)} + \boldsymbol{\Phi}_{21}\boldsymbol{W}^{(1)}\boldsymbol{Y}_{(t-2)} + \boldsymbol{e}_t \tag{9}$$

$$\text{GSTAR}(1;1,2) \quad : \boldsymbol{Y}_t = \boldsymbol{\Phi}_{10}\boldsymbol{Y}_{(t-1)} + \boldsymbol{\Phi}_{11}\boldsymbol{W}^{(1)}\boldsymbol{Y}_{(t-1)} + \boldsymbol{\Phi}_{12}\boldsymbol{W}^{(2)}\boldsymbol{Y}_{(t-2)} + \boldsymbol{e}_t \tag{10}$$

$$\text{GSTAR}(2;1,2) \quad : \boldsymbol{Y}_t = \boldsymbol{\Phi}_{10}\boldsymbol{Y}_{(t-1)} + \boldsymbol{\Phi}_{11}\boldsymbol{W}^{(1)}\boldsymbol{Y}_{(t-1)} + \boldsymbol{\Phi}_{12}\boldsymbol{W}^{(2)}\boldsymbol{Y}_{(t-2)} + \boldsymbol{\Phi}_{20}\boldsymbol{Y}_{(t-2)} + \boldsymbol{\Phi}_{21}\boldsymbol{W}^{(1)}\boldsymbol{Y}_{(t-2)} + \boldsymbol{e}_t \tag{11}$$

Residual diagnostic tests for all model configurations are presented in Table 3. Specifically, the table reports the diagnostic results for the GSTAR(1;1) model with areal representation

using three spatial weight schemes Queen, Rook, and IDW. It also includes the diagnostic outcomes for the GSTAR(2;1,2) model applied to the $\mathbf{1.00}° \times \mathbf{1.00}°$ grid representation using the same spatial weighting schemes. These diagnostic evaluations are used to assess model adequacy, particularly regarding residual normality, independence, and the presence of remaining spatial–temporal autocorrelation (Dare et al., 2022). In the table, a check mark (✓) indicates that the residuals satisfy the normality and independence assumptions, whereas a cross mark (×) indicates that the assumptions are not met.

Table 3. Residual diagnostic 3 results for the GSTAR($\boldsymbol{p}$; $\boldsymbol{\lambda}_1, \boldsymbol{\lambda}_2, \ldots, \boldsymbol{\lambda}_p$) models

Model	Queen Contiguity			Rook Contiguity			IDW		
	RMSE	**Ind.**	**Norm.**	**RMSE**	**Ind.**	**Norm.**	**RMSE**	**Ind.**	**Norm.**
GSTAR (1;1)									
Areal	7.423	✓	✓	7.423	✓	✓	6.671	✓	×
Grid (0.50° × 0.50°)	4.551	✓	×	4.615	✓	×	4.978	✓	×
Grid (1.00° × 1.00°)	7.529	✓	✓	6.866	✓	✓	6.866	✓	✓
Grid (1.25° × 1.25°)	7.290	×	×	7.290	×	×	7.290	×	×
⋮	⋮	⋮	⋮	⋮	⋮	⋮	⋮	⋮	⋮
GSTAR (2;1,2)									
Areal	10.790	✓	×	10.790	✓	×	11.532	✓	×
Grid (0.50° × 0.50°)	7.391	✓	×	6.510	✓	×	6.089	✓	×
Grid (1.00° × 1.00°)	10.512	✓	×	12.110	✓	✓	11.330	✓	✓

Based on the results of the third-stage residual diagnostic presented in Table 4, the GSTAR (1;1) model with a Grid (1.00° × 1.00°) spatial structure and the Rook and IDW spatial weight matrices satisfies the assumptions of normality and residual independence. The residuals at all locations are independent (Ind. = ✓) and follow a normal distribution (Norm. = ✓), and the model produces a Root Mean Square Error (RMSE) of 6.866, which is the lowest among the models tested. Furthermore, the parameters of the GSTAR (1;1) model with Grid (1.00° × 1.00°) using Rook and IDW spatial weights were tested for significance in three stages. The results indicate that all temporal and spatial parameters for both weight matrices meet the significance criteria, confirming the model's validity for predicting FRP hotspots in forest fires in the study area. The Rook and IDW parameters after three-stage significance testing are as follows.

$$\boldsymbol{\Phi}_{10} = diag(\mathbf{0.000}, -0.472\,, \mathbf{0.000}, \mathbf{0.000}, \mathbf{0.000}, \mathbf{0.000}, \mathbf{0.000}, \mathbf{0.000})$$
$$\boldsymbol{\Phi}_{11} = diag(0.091\,, 0.429, 0.060, \mathbf{0.000}, \mathbf{0.000}, -0.109, \mathbf{0.000}, -0.454)$$

The values on the diagonal indicate the contribution of each location to the temporal and spatial components in the model. Parameters with a zero value (**0.000**, shown in bold) indicate that the effect at that location is not significant and can be ignored in the estimation process. Considering the diagnostic results and the estimated parameters, the GSTAR(1;1) model with

model with a Grid (1.00° × 1.00°) structure and Rook and IDW spatial weight matrices is deemed appropriate for analyzing and predicting forest fire patterns.

6. Selection of Best Grid

The diagnostic test results indicate that the combination of a Grid (1.00° × 1.00°) spatial structure with Rook and IDW spatial weight matrices yields the best performance, with a Root Mean Square Error (RMSE) of 6.866, the lowest among the evaluated models. This result demonstrates high predictive accuracy and indicates that the model effectively captures the patterns and dynamics of forest fire hotspots. Accordingly, the GSTAR(1;1) model with Rook and IDW spatial weight matrices under the Grid (1.00° × 1.00°) structure can be expressed as follows.

$$
\begin{aligned}
\hat{Y}_t^{(1)} &= 0{,}046\, Y_{(t-1)}^{(2)} + 0{,}046\, Y_{(t-1)}^{(3)} \\
\hat{Y}_t^{(2)} &= 0{,}215\, Y_{(t-1)}^{(1)} - 0{,}472\, Y_{(t-1)}^{(2)} + 0{,}215\, Y_{(t-1)}^{(4)} \\
\hat{Y}_t^{(3)} &= 0{,}020\, Y_{(t-1)}^{(1)} + 0{,}020\, Y_{(t-1)}^{(4)} + 0{,}020\, Y_{(t-1)}^{(5)} \\
&\vdots \\
\hat{Y}_t^{(8)} &= -0{,}227\, Y_{(t-1)}^{(6)} - 0{,}227\, Y_{(t-1)}^{(7)}
\end{aligned}
$$

Based on the established model equation, the Influence of neighboring locations on the primary location can be examined. For example, according $\hat{Y}_t^{(1)}$, the predicted value at time period t for grid A_1 is affected by the values at time period $(t-1)$ from other grids. Grids A_2 and A_3 exert a positive Influence of 0.046. This indicates that the predicted value for grid A_1 is influenced not only by its own historical data but also by data from neighboring grids at previous time periods, with varying levels of contribution across grids. Negative parameter estimates in the GSTAR model used to predict FRP across grids in the study area may be attributed to seasonal effects influencing forest fire patterns. FRP values tend to increase during the dry season due to low rainfall and high temperatures, while they generally decrease during the rainy season. If the GSTAR model does not fully capture this seasonal pattern, the relationship between FRP values in the previous period $(t-1)$ and the current period (t) may be negative. In addition, differences in the onset of the rainy season across grids can lead to negative spatial relationships, particularly when FRP values in one grid begin to decline due to earlier rainfall. In contrast, neighboring grids still exhibit relatively high FRP values. Consequently, negative parameter estimates in the GSTAR model reflect the Influence of seasonal factors and heterogeneous forest fire dynamics across grids that the model does not fully accommodate.

7. Forecast

The GSTAR(1;1) model with a Grid 1.00 × 1.00 spatial structure and Rook and IDW spatial weight matrices is used to forecast FRP values for the next four weeks at each grid location and can be seen in Table 4.

Table 4. Result Prediction of FRP Maximum for Each Location

Week	September							
	A_1	A_2	A_3	A_4	A_5	A_6	A_7	A_8
Week 62	146.41	42.07	323.50	167.40	280.29	240.82	62.03	65.91
Week 63	145.41	57.32	323.76	167.40	280.29	242.61	62.03	69.23
Week 64	146.12	49.90	323.74	167.40	280.29	242.49	62.03	68.82
Week 65	145.78	53.55	323.75	167.40	280.29	242.51	62.03	68.85

Based on Table 4, the predicted FRP values for locations $A_1 - A_8$ over four weeks in September are presented. In general, the predicted FRP values at several locations exhibit variations across weeks, reflecting the Influence of temporal lag and spatial effects from neighboring locations in accordance with the significant parameters of the model. However, the predicted FRP values at locations A_4, A_5, and A_7 remain constant across all weeks. This is because the parameters associated with these locations do not meet the significance criteria and were therefore set to zero. As a result, temporal dynamics and spatial influences at locations A_4, A_5, and A_7 do not contribute to the model, leading to identical FRP predictions for these locations across all forecast periods. The comparison between actual and predicted FRP values at several locations in September 2025 is presented in the following figures, as shown in Figure 8. The graphs illustrate the temporal pattern of FRP, with actual values shown in orange and model estimates in blue.

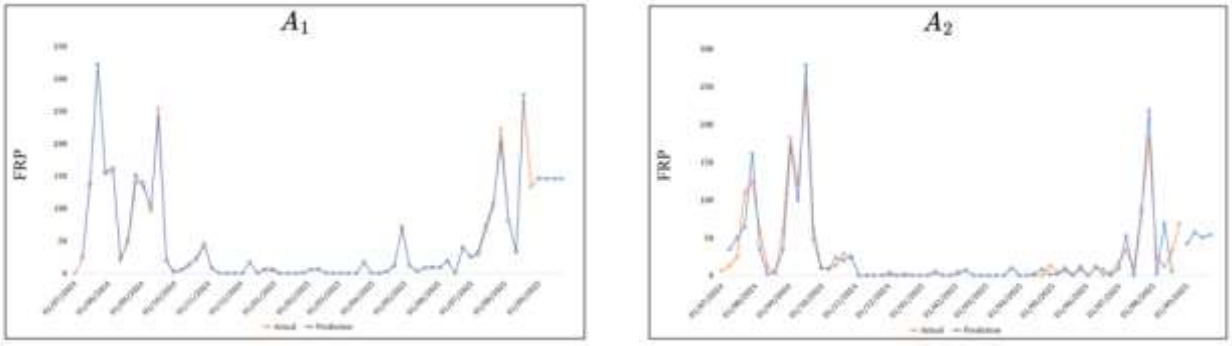

(a) (b)

Figure 8. Comparison Plot of the Actual, Estimation, and Forecast Values for each Location (a) A_1 (b) A_2

As shown by the strong correspondence between the estimated line and the actual data at most locations, Figure 8 demonstrates that the model accurately represents the actual data pattern. In general, the predictions closely follow the primary trend of the actual data across many observation points, although some deviations persist at specific locations. This indicates that the model performs reasonably well overall but still requires further refinement to improve prediction accuracy in certain area.

D. CONCLUSION

GSTAR modeling was conducted by considering four spatial partitions, namely an areal structure and grid combinations with sizes of 0.50° × 0.50°, 1.00° × 1.00°, and 1.25° × 1.25°, as well as three types of spatial weight matrices: Queen Contiguity, Rook Contiguity, and Inverse

Distance Weight (IDW). The evaluation results indicate that the GSTAR(1;1) model with a $1.00° \times 1.00°$ grid and Rook Contiguity and IDW spatial weight matrices is the best-performing model. At the first spatial lag, both weight matrices yield the same spatial structure, leading to comparable model performance. The selected GSTAR(1;1) model satisfies the white noise assumption based on the third-stage diagnostic test and yields an RMSE value of 6.866, which is the lowest among the evaluated models. A lower RMSE indicates a smaller discrepancy between predicted and actual values, implying higher predictive accuracy. The $1.00° \times 1.00°$ grid divides the study area into eight locations $(A_1 - A_8)$, which is considered efficient for representing spatial variation without generating an excessive number of locations.

The parameter estimation results indicate that FRP values Influence forest fire occurrences at a given location in the previous period and that spatial effects from neighboring locations also Influence them. Several locations exhibit statistically insignificant parameters that were set to zero, resulting in constant predicted values across weeks. Overall, the forecasting results show a decreasing trend in FRP hotspot values from the first to the fourth week of September 2025, which is presumed to be influenced by environmental factors, notably the transition from the dry season to the rainy season, suggesting that the model results can support early and targeted forest fire mitigation planning in high-risk areas.

REFERENCES

Abdullah, A. S., Matoha, S., Lubis, D. A., Falah, A. N., Jaya, I. G. N. M., Hermawan, E., & Ruchjana, B. N. (2018). Implementation of Generalized Space Time Autoregressive (GSTAR)-Kriging model for predicting rainfall data at unobserved locations in West Java. *Applied Mathematics and Information Sciences*, *12*(3), 607–615. https://doi.org/10.18576/amis/120316

Aprianti, A., Faulina, N., & Usman, M. (2024). Generalized Space Time Autoregressive (GSTAR) Model for Air Temperature Forecasting in the South Sumatera, Riau, and Jambi Provinces. *InPrime: Indonesian Journal of Pure and Applied Mathematics*, *6*(1), 1–13. https://doi.org/10.15408/inprime.v6i1.36049

Ayyash, M. Y., Huda, N. M., & Imro'ah, N. (2025). The GSTAR (1;1) Modelling with Three Combination of the Grid Sizes and Spatial Weight Matrix in Forest Fires Cases. *JTAM (Jurnal Teori Dan Aplikasi Matematika)*, *9*(1), 134–146. https://doi.org/10.31764/jtam.v9i1.27543

Cahyono, S. A., P Warsito, S., Andayani, W., & H Darwanto, D. (2015). Faktor-Faktor Yang Mempengaruhi Kebakaran Hutan Di Indonesia Dan Implikasi Kebijakannya. *Jurnal Sylva Lestari*, *3*(1), 103. https://doi.org/10.23960/jsl13103-112

Dare, J., Patrick, A. O., & Oyewola, D. O. (2022). Comparison of Stationarity on Ljung Box Test Statistics for Forecasting. *Earthline Journal of Mathematical Sciences*, *8*(2), 325–336. https://doi.org/10.34198/ejms.8222.325336

Hestuningtias, F., & Kurniawan, M. H. S. (2023). The Implementation of the Generalized Space-Time Autoregressive (GSTAR) Model for Inflation Prediction. *Enthusiastic : International Journal of Applied Statistics and Data Science*, *3*(2), 176–188. https://doi.org/10.20885/enthusiastic.vol3.iss2.art5

Huda, N. M., & Imro'ah, N. (2023). Determination of the best weight matrix for the Generalized Space Time Autoregressive (GSTAR) model in the Covid-19 case on Java Island, Indonesia. *Spatial Statistics*, *54*, 100734. https://doi.org/10.1016/j.spasta.2023.100734

Huda, N. M., & Imro'ah, N. (2024). Covid-19 case modeling in Java Island using a spatial model, GSTAR(1;1), with modified spatial weights: Queen contiguity weight matrix. *AIP Conference Proceedings*, *2891*(1), 090009. https://doi.org/10.1063/5.0201676

Huda, N. M., Imro'ah, N., Arini, N. F., Utami, D. S., & Umairah, T. (2023). Looking at GDP from a Statistical Perspective: Spatio-Temporal GSTAR(1;1) Model. *JTAM (Jurnal Teori Dan Aplikasi Matematika)*, *7*(4), 976–988. https://doi.org/10.31764/jtam.v7i4.16236

Huda, N. M., Mukhaiyar, U., & Pasaribu, U. S. (2021). The approximation of GSTAR model for discrete cases through INAR model. *Journal of Physics: Conference Series*, *1722*(1), 012100. https://doi.org/10.1088/1742-6596/1722/1/012100

Imro'ah, N., Huda, N. M., Pratiwi, H., & Ayyash, M. Y. (2025). A Hybrid ARIMA-Intervention Modelling for Forest Fire Risk in The Dry Season. *CAUCHY: Jurnal Matematika Murni Dan Aplikasi*, *10*(2), 957–969. https://doi.org/10.18860/cauchy.v10i2.36741

Jalilov, S.-M., Rochmayanto, Y., Hidayat, D. C., Raharjo, J. T., Mendham, D., & Langston, J. D. (2025). Unveiling economic dimensions of peatland restoration in Indonesia: A systematic literature review. *Ecosystem Services*, *71*, 101693. https://doi.org/10.1016/j.ecoser.2024.101693

Kusuma, V. M. A., Furqon, M. T., & Muflikhah, L. (2017). Implementasi metode fuzzy subtractive clustering untuk pengelompokan data potensi kebakaran hutan/lahan. *Jurnal Pengembangan Teknologi Informasi Dan Ilmu Komputer*, *1*(9), 876–884. https://j-ptiik.ub.ac.id/index.php/j-ptiik/article/view/271

Mubarak, F., Aslanargun, A., & Sıklar, I. (2021). High Order Spatial Weighting Matrix Using Google Trends. *International Journal of Research and Review*, *8*(11), 388–396. https://doi.org/10.52403/ijrr.20211150

Mukhaiyar, U., Bilad, B. I., & Pasaribu, U. S. (2021). The Generalized STAR Modelling with Minimum Spanning Tree Approach of Weight Matrix for COVID-19 Case in Java Island. *Journal of Physics: Conference Series*, *2084*(1), 012003. https://doi.org/10.1088/1742-6596/2084/1/012003

Mukhaiyar, U., Mahdiyasa, A. W., Prastoro, T., Suherlan, B. C., Pasaribu, U. S., & Indratno, S. W. (2024). Spatial and Time Series Modelling for the Groundwater Level of Peatlands in Riau and Central Kalimantan, Indonesia. In W. F. Wan Yaacob, Y. B. Wah, & O. U. Mehmood (Eds.), *Decision Mathematics, Statistical Learning and Data Mining* (pp. 89–104). Springer Nature. https://doi.org/10.1007/978-981-97-3450-4_7

NASA-FIRMS. (2025, September 1). *NASA-FIRMS*. https://firms.modaps.eosdis.nasa.gov/map/

Notonegoro, Y., Andriyana, Y., & Ruchjana, B. (2024). Comparison of distance-based spatial weight matrix in modeling Internet signal strengths in Tasikmalaya regency using logistic spatial autoregressive model. *International Journal of Data and Network Science*, *8*(2), 893–906. https://doi.org/10.5267/j.ijdns.2023.12.016

Nurhayati, N., Hamidi, M. R., Mukhaiyar, U., & Sari, K. N. (2025). Cross-Correlation Analysis in Evaluating Spatio-Temporal Data Dependence of Climate Variables Through the GSTAR Model. *Jurnal Matematika, Statistika Dan Komputasi*, *21*(3), 813–831. https://doi.org/10.20956/j.v21i3.43665

Omar, M. S., Ifandi, E., Sukri, R. S., Kalaitzidis, S., Christanis, K., Lai, D. T. C., Bashir, S., & Tsikouras, B. (2022). Peatlands in Southeast Asia: A comprehensive geological review. *Earth-Science Reviews*, *232*, 104149. https://doi.org/10.1016/j.earscirev.2022.104149

Pasaribu, U., Mukhaiyar, U., & Heriawan, M. (2018). Spatial weight determination of GSTAR (1; 1) model by using kernel function. *Journal of Physics: Conference Series, 1028*(1), 012223. https://doi.org/10.1088/1742-6596/1028/1/012223

Pasaribu, U. S., Mukhaiyar, U., Heriawan, M. N., & Yundari, Y. (2022). Generalized Space-Time Autoregressive Modeling of the Vertical Distribution of Copper and Gold Grades with a Porphyry-Deposit Case Study. *International Journal on Advanced Science, Engineering and Information Technology*, *12*(5), 2030–2038. https://doi.org/10.18517/ijaseit.12.5.14835

Pasaribu, U. S., Mukhaiyar, U., Huda, N. M., Sari, K. N., & Indratno, S. W. (2021). Modelling COVID-19 growth cases of provinces in java Island by modified spatial weight matrix GSTAR through railroad passenger's mobility. *Heliyon*, *7*(2), e06025. https://doi.org/10.1016/j.heliyon.2021.e06025

Pratiwi, H., Imro'ah, N., & Huda, N. M. (2025). Forest Fire Analysis From Perspective Of Spatial-Temporal Using Gstar (p;λ_1,λ_2,…,λ_p) Model. *BAREKENG: Jurnal Ilmu Matematika Dan Terapan*, *19*(2), Article 2. https://doi.org/10.30598/barekengvol19iss2pp1379-1392

Pratiwi, H., Imro'ah, N., Huda, N. M., & Ayyash, M. Y. (2025). Comparison Of Weight Matrix In Hotspot Modeling In West Kalimantan Using The Gstar Method. *Jurnal Matematika UNAND*, *14*(1), 31–45. https://doi.org/10.25077/jmua.14.1.31-45.2025

Purwaningsih, T., Winarko, E., & Mustofa, K. (2025). Enhancing Accuracy of Spatiotemporal Model Estimation Using Modified Binary Distance Spatiotemporal Weight Matrix. *International Journal of Intelligent Engineering & Systems*, *18*(8), 383–397. https://doi.org/10.22266/ijies2025.0930.24

Pusporani, E., Yuniar, M. A. D. P., Fajrina, S. A. N., Alexandra, V. A., & Mardianto, M. F. F. (2024). Generalized Space Time Autoregressive (GSTAR) Modeling in Predicting the Price of Bird's Eye Chili in East Java, West Java, and Central Java. *CAUCHY: Jurnal Matematika Murni Dan Aplikasi*, *9*(2), Article 2. https://doi.org/10.18860/ca.v9i2.25730

Ray, T., Malasiya, D., Verma, A., Purswani, E., Qureshi, A., Khan, M. L., & Verma, S. (2023). Characterization of spatial–temporal distribution of forest fire in Chhattisgarh, India, using MODIS-based active fire data. *Sustainability*, *15*(9), 7046. https://doi.org/10.3390/su15097046

Roza, A., Violita, E. S., & Aktivani, S. (2022). Study of Inflation using Stationary Test with Augmented Dickey Fuller & Phillips-Peron Unit Root Test (Case in Bukittinggi City Inflation for 2014-2019). *EKSAKTA: Berkala Ilmiah Bidang MIPA*, *23*(02), Article 02. https://doi.org/10.24036/eksakta/vol23-iss02/303

Setiawan, S., Wahyuningrum, S. R., & Akbar, M. S. (2016). GSTARX-GLS model for spatio-temporal data forecasting. *Malaysian Journal of Mathematical Sciences*, *10*, 91–103. https://scholar.its.ac.id/en/publications/gstarx-gls-model-for-spatio-temporal-data-forecasting/

sipongi.menlhk.go.id. (2025, September 1). *Sipongi.menlhk.go.id*. https://sipongi.menlhk.go.id/

Umer, U. M., Sevil, T., & Sevil, G. (2018). Forecasting performance of smooth transition autoregressive (STAR) model on travel and leisure stock index. *The Journal of Finance and Data Science*, *4*(2), 90–100. https://doi.org/10.1016/j.jfds.2017.11.006

Utami, R., Mukhaiyar, U., Mardiyah, N., Sa'adah, Y., & Widyawati, E. (2024). Spatial Weighting Selection in GSTAR and S-GSTAR Models for Temperature Prediction. *Jurnal Matematika, Statistika Dan Komputasi*, *20*(3), Article 3. https://doi.org/10.20956/j.v20i3.34305

Yundari, Pasaribu, U. S., Mukhaiyar, U., & Heriawan, M. N. (2018). Spatial Weight Determination of GSTAR(1;1) Model by Using Kernel Function. *Journal of Physics: Conference Series*, *1028*(1), 012223. https://doi.org/10.1088/1742-6596/1028/1/012223

Yundari, Y., Rahmawati, A., & Pratiwi, Y. E. (2025). GSTAR (1;1) Transfer Function Model for Forecasting Chili Prices with Rainfall Effect. *ZERO: Jurnal Sains, Matematika Dan Terapan*, *9*(2), 511–523. https://doi.org/10.30829/zero.v9i2.26119